Chemical Engineering Science 122 (2015) 185–196

Contents lists available at ScienceDirect

Chemical Engineering Science

journal homepage: www.elsevier.com/locate/ces

Dissipative particle dynamics study of the water/benzene/caprolactam system in the absence or presence of non-ionic surfactants

Kaihang Shi [a,b], Cheng Lian [a], Zhishan Bai [c], Shuangliang Zhao [a,*], Honglai Liu [a]

[a] State Key Laboratory of Chemical Engineering, East China University of Science and Technology, Shanghai 200237, China
[b] Department of Polymer Materials and Engineering, School of Material Science and Engineering, East China University of Science and Technology, Shanghai 200237, China
[c] State Environmental Protection Key Laboratory of Environmental Risk Assessment and Control on Chemical Process, East China University of Science and Technology, Shanghai 200237, China

HIGHLIGHTS

- The benzene/water interfacial tension with caprolactam is quantitatively predicted.
- Caprolactam (CPL) at the benzene/water interface improves the surfactant efficiency.
- With CPL at interface surfactant efficiency does not always increase with tail length.
- The addition of surfactants drives CPL from water/benzene interface to water phase.

ARTICLE INFO

Article history:
Received 25 May 2014
Received in revised form
14 September 2014
Accepted 16 September 2014
Available online 23 September 2014

Keywords:
Caprolactam
Benzene
Extraction
Surfactant
Interface
Dissipative particle dynamics

ABSTRACT

A dissipative particle dynamics (DPD) simulation is performed to study the properties of water/benzene/caprolactam (W/B/CPL) system in the absence or presence of different non-ionic surfactants. The interaction parameters involved in the constructed coarse-grained model are determined by combining two solubility-parameter models and all-atom molecular dynamics. By using the DPD method, we first show that the interfacial tensions in the W/B/CPL system can be quantitatively predicted and compared with available experimental and other theoretical data. Secondly, by calculating the density profile of CPL and the efficiency of the surfactant at various conditions, we demonstrate that (i) unlike Traube's rule, the efficiency of the surfactant does not always improve with an increase in its hydrophobic tail length, and due to the accumulation of CPL at the interface, this tail length effect becomes nearly negligible when the tail is long; (ii) CPL, like a weak surfactant, is capable of activating surfactants at the interface by improving the efficiency of surfactant; and (iii) the addition of surfactants (especially with short tail lengths) into the W/B/CPL system can drive CPL into the water-rich phase, which can be applied to the design of more efficient industrial extraction process for recycling CPL.

1. Introduction

Caprolactam (CPL) is an important organic chemical raw material, mainly used to produce polyamide 6 engineering plastic and synthetic fibers. It also has extensive applications in medical engineering for the production of antiplatelet 6-aminocaproic acid, etc. The worldwide production of caprolactam is approximately 4.5 billion kilograms per year (Ullmann's Encyclopedia of Industrial Chemistry, 2000). However, current production generally requires a long, multi-step, multi-device process that results in large consumption of raw materials and difficulty in separating caprolactam from the intermediate products and byproducts. Distilled benzene (B) residue contains approximately 20–50% caprolactam ingredients, which greatly decreases the efficiency of the entire production process. Recently, a new technique (Dsinter-De Hondt and Lemmens, 2004; Vandelden et al., 2006) was designed to recycle caprolactam from benzene residue using a water flow, which takes advantage of the lower price of water and high solubility of caprolactam in it; the remaining challenge is to improve the extraction efficiency.

The extraction efficiency of caprolactam from benzene with water is not only determined by the bulk equilibrium properties but also associated with the local properties near the organic–aqueous interface. The bulk equilibrium of the water/benzene/caprolactam (W/B/CPL) system has been studied experimentally (Vandelden et al., 2006; Wijtkamp et al., 1999). The interfacial

* Corresponding author.
E-mail address: szhao@ecust.edu.cn (S. Zhao).

http://dx.doi.org/10.1016/j.ces.2014.09.030
0009-2509/

tension of the W/B/CPL system was also measured by van Delden et al. (2004). Theoretical studies of the W/B/CPL system were carried using self-consistent field theory (SCFT) (Tuinier and Krooshof, 2012) and gave reasonable predictions of the interfacial properties, including interfacial tension and local concentration profiles near the interface.

The interfacial properties of multi-component systems are usually modified by the addition of surfactants. For instance, amphiphilic surfactants can stabilize the water/oil interface and the characteristics of chemical structure, temperature and concentration would enable them to form various morphologies both at the interface and in the bulk phase; these different phase behaviors of the surfactants change the interfacial properties of the system (interfacial tension, interfacial thickness, etc.). In the extraction process of caprolactam from benzene, non-ionic surfactants also play a significant role in complex systems, as we show in present study. In recent decades, a large number of theoretical investigations have been dedicated to studying the properties of surfactants in water/oil systems using dissipative particle dynamics (DPD) (Rekvig et al., 2003; Li et al., 2011; Ginzburg et al., 2011; Luu et al., 2013), Monte Carlo simulations (MC) (Rekvig et al., 2003; Larson, 1992), SCFT (Ginzburg et al., 2011), and density functional theory (Emborsky et al., 2011; Marshall et al., 2012). Many experimental techniques have also been applied to investigate the self-assembly and other phase behaviors of surfactants, such as neutron scattering experiments (Lu et al., 2000; Aswal et al., 2001), small angle light scattering (Richtering et al., 1994), fluorescence labeling (Lin et al., 2003) and X-ray surface scattering (Schlossman and Tikhonov, 2008). However, there are few theoretical investigations of surfactants in ternary system, for example, the water/benzene/caprolactam system.

It is in principal viable to study the behavior of surfactants at the atomistic level using molecular dynamics (MD). MD can provide specific information about the behavior of surfactants in the system without losing atomistic details. However, the time scale and length scale accessible to classical MD are too short to allow for observation of the diffusion of surfactants and caprolactam in the water/benzene system. By combing two or three fragments or several polymer molecules into one coarse-grained bead, a coarse-grained simulation allows for the study of larger systems and larger time scales up to the mesoscopic level. Unsurprisingly, this process loses atomistic information. While different simulation methods have different merits, the choice should always serve the research purpose.

The research purpose of this work is to study the quantitative properties of the water/benzene/caprolactam system with or without non-ionic surfactants, and due to the complexity of the system, the dissipative particle dynamics (DPD) technique (Hoogerbrugge and Koelman, 1992; Español and Warren, 1995; Groot and Warren, 1997) is applied. We first construct a coarse-grained model from the different components, and then, the parameters in this model, e.g., the Flory–Huggins binary interaction parameters, are derived using both the Hildebrand solubility parameter and the Hansen solubility parameter. Next, we validate our coarse-grained model by calculating the interfacial tensions of water/benzene interface with the presence of CPL (i.e., the ternary system in the absence of surfactants), and then comparing our simulation predictions with the corresponding experimental data and other available theoretical results. The comparisons at different CPL mass fractions are quantitatively good, which justifies our coarse-grained model. Using this coarse-grained model, we then extend our study to ternary systems through the addition of non-ionic surfactants.

The remainder of this article is organized as follows: in Section 2, we recall the DPD method and construct the coarse-grained model system. The determination of the parameters for the model systems is also described. In Section 3, we study the ternary system of water/benzene/CPL without surfactant, and the simulation results are presented and compared with available sources. In the second part of this section, we move to a ternary system through the addition of various surfactants. Finally, in Section 4, we give a brief conclusion.

2. Modeling and methods

2.1. Dissipative particle dynamics simulation

Dissipative particle dynamics (DPD) is a coarse-grained simulation method in which a complex molecule, such as a polymer or surfactant, is represented by soft spherical beads joined with springs. The interaction is usually described through simple and pairwise-additive potentials. Unlike SCF theory, DPD allows one to study not only the equilibrium thermodynamic properties but also the dynamic properties and the time-dependent evolution of the structure (Ginzburg et al., 2011).

Similar to MD simulation, particle positions and velocities in DPD are governed by Newtonian law of motion:

$$\frac{d\mathbf{r}_i}{dt} = \mathbf{v}_i \tag{1a}$$

$$m_i \frac{d\mathbf{v}_i}{dt} = \mathbf{F}_i \tag{1b}$$

where $\mathbf{r}_i$, $\mathbf{v}_i$ and m_i are the position, velocity and mass of the ith bead, respectively, and $\mathbf{F}_i$ is the total force exerted upon it. The total force is the sum of the conservative force ($\mathbf{F}_{ij}^C$), dissipative force ($\mathbf{F}_{ij}^D$) and random force ($\mathbf{F}_{ij}^R$):

$$\mathbf{F}_i = \sum_{i \neq j} (\mathbf{F}_{ij}^C + \mathbf{F}_{ij}^D + \mathbf{F}_{ij}^R) \tag{2}$$

The first term on the RHS of above equation represents a conservative force between the ith particle and the jth particle, which is usually written in the soft repulsion form:

$$\mathbf{F}_{ij}^C = \begin{cases} a_{ij}(1 - r_{ij}/r_c)\hat{\mathbf{r}}_{ij} & (r_{ij} < r_c) \\ 0 & (r_{ij} \geq r_c) \end{cases} \tag{3}$$

where $r_{ij} = r_i - r_j$ is the distance between the ith and the jth bead. $\hat{\mathbf{r}}_{ij}$ is the unit vector denoting the direction from bead i to j. r_c is a cut-off radius, and it gives the extent of the interaction range between a pair of beads. The coefficient a_{ij} is a parameter expressing the maximum repulsion between the ith and the jth bead, and it can be calculated from the Flory–Huggins binary interaction parameter, χ_{ij}, using the relation below for $\rho r_c^3 = 3$ as shown in Ref. Groot and Warren (1997):

$$a_{ij} = (a_{ii} + 3.27\chi_{ij})(k_B T / r_c) \tag{4}$$

Here k_B is the Boltzmann constant, and T is the absolute temperature. The dimensionless parameter χ_{ij} involved in Eq. (4) can be calculated from the solubility parameters, which we will discuss later.

The other two forces in Eq. (2) are the dissipative force ($\mathbf{F}_{ij}^D$), which follows:

$$\mathbf{F}_{ij}^D = -\eta w^D(r_{ij})(\hat{\mathbf{r}}_{ij} \cdot \mathbf{v}_{ij})\hat{\mathbf{r}}_{ij} \tag{5}$$

and the random force ($\mathbf{F}_{ij}^R$):

$$\mathbf{F}_{ij}^R = \sigma w^R(r_{ij})\zeta_{ij}\Delta t^{-1/2}\hat{\mathbf{r}}_{ij} \tag{6}$$

In the Eq. (5), $\mathbf{v}_{ij} = \mathbf{v}_i - \mathbf{v}_j$ is the difference between the velocity of the ith bead and the jth bead, η is the friction coefficient, and as in Eq. (6), σ is the amplitude of the noise. ζ_{ij} is a random number between 0 and 1 and subjected to a uniform distribution for

simplicity; it is statistically independent from the pair of beads. Δt is the time step with which the equations of motion (Eqs. (1a) and (1b)) are solved. $w^D(r_{ij})$ and $w^R(r_{ij})$ are the weight functions. The combination of both forces leads to a thermostat that conserves the total momentum of the system.

To obey the fluctuation-dissipation theorem, the weight functions of the dissipative force and random force should satisfy:

$$w^D(r_{ij}) = [w^R(r_{ij})]^2 \tag{7}$$

$$\sigma^2 = 2\eta k_B T \tag{8}$$

where

$$w^R(r_{ij}) = \begin{cases} 1 - \frac{r_{ij}}{r_c} & (r_{ij} < r_c) \\ 0 & (r_{ij} \geq r_c) \end{cases} \tag{9}$$

Throughout our work, we use reduced DPD units during our simulation. In specific, we take r_c as the unit of length and k_BT as the unit of energy. The masses of all of the beads are set equal (m in our calculation). Based on these factors, the unit of time, τ, can be determined by

$$\tau = r_c\sqrt{m/k_BT} \tag{10}$$

2.2. Models and interaction parameters

The DPD simulation is a mesoscopic approach that relies on the construction of a coarse-grained model. The coarseness of the grain can affect the computational accuracy of the interfacial tension. An unsuitably coarse-grained model would result in a large deviation of the simulation results (Maiti and McGrother, 2004). In our work, we group five water molecules as one DPD particle, and this grouping has already been confirmed to produce ideal interfacial tensions (Maiti and McGrother, 2004; Lin et al., 2012). One benzene molecule and one caprolactam molecule are represented by two individual DPD particles. The non-ionic surfactant molecule is modeled with a bead-chain composed of a hydrophilic head group and m hydrophobic tail groups; these groups are connected by a harmonic spring (Rekvig et al., 2003):

$$\mathbf{F}_{ij}^{bond} = -k_s(r_{ij} - r_0)\hat{\mathbf{r}}_{ij} \tag{11}$$

The spring constant is set as $k_s = 100$ and the equilibrium distance at $r_0 = 0.7$. For simplicity, we denote water bead, benzene bead, caprolactam bead, head group, and tail group of the surfactant with the shorthand notations W, B, CPL, H and T, respectively. The coarse-grained models for each component are schematically depicted in Fig. 1.

Now, we return to the determination of χ_{ij}. As mentioned above, the interaction parameter a_{ij} can be calculated using the Flory–Huggins parameter χ_{ij} between the components i and j using Eq. (4). If we assume that the heat of mixing in this case obeys the Hildebrand–Scatchard regular solution theory (Scatchard, 1931; Hildebrand and Wood, 1933), the parameter χ_{ij} can then be determined from the Hildebrand solubility parameters $\delta_i(T)$ and $\delta_j(T)$.

$$\chi(T)_{ij} = \frac{V_{ij}}{RT}(\delta_i(T) - \delta_j(T))^2 \tag{12}$$

Here R is the gas constant and V_{ij} is the partial molar volume. In DPD, the nearest equivalent of a partial molar volume is the volume associated with a DPD bead, and in our calculation, we replace the partial molar volume, V_{ij}, by the average molar volume of the two involved beads (Lin et al., 2012). Although Eq. (12) applies only to non-polar systems, it appears to be a good approximation for the water/benzene binary system (Mayoral and Goicochea, 2013) in the sense that this approximation can satisfactorily predict the interfacial tension compared with experimental results.

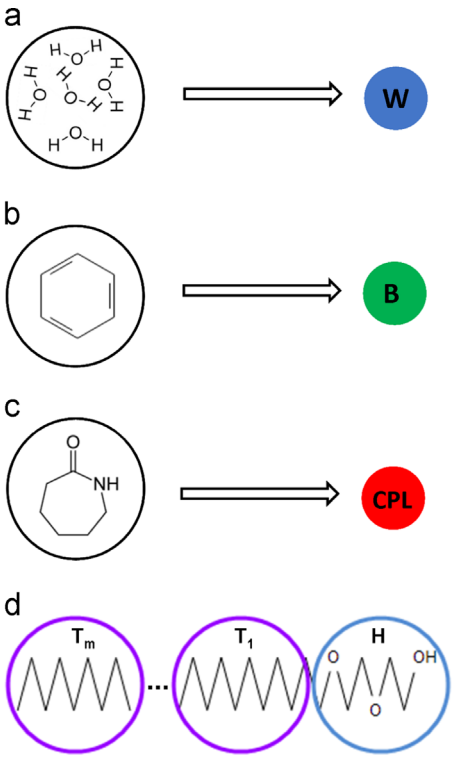

Fig. 1. Schematic description of the coarse-grained models for (a) water (W), (b) benzene (B), (c) caprolactam (CPL), and (d) amphiphilic surfactant HT_m.

Table 1
Molecular volumes and solubility parameters (δ) for water and benzene at 293 K calculated using atomistic molecular dynamics. The experimental results are shown for comparison.

Molecule	$V_{molecule}$ (Å^3)	Solubility parameter δ at 293 K (J/cm^3)$^{1/2}$	Exp. solubility parameter δ at 298 K (J/cm^3)$^{1/2}$ (Barton, 1975)
Water	29.91	47.18	47.9
Benzene	145.775	19.52	18.8

The values of the Hildebrand solubility parameters can be determined using all-atom molecular dynamics(AAMD) (Lin et al., 2012; Mayoral and Goicochea, 2013). To calculate the Hildebrand solubility parameter δ, periodic cells of amorphous fluid structures are constructed using the Amorphous Cell module of the *Materials Studio* suite (Materials Studio, Accelrys, 2014). The simulation box contains 100 molecules of water or benzene with total atomistic details. The atomistic models for water and benzene as well as the interactions between the atoms are taken from the COMPASS force field (Sun, 1998). The *Discover* engine is used to equilibrate the system at 293 K for a total of 2×10^5 steps in an *NPT* ensemble. The resulting solubility parameters are comparable to the experimental data (Barton, 1975), indicating good consistency. The final solubility parameters are shown in Table 1.

However, Eq. (12) cannot be directly applied to polar systems, such as the water/caprolactam and benzene/caprolactam systems, due to the non-negligible polar force and hydrogen bond effect between the molecules. Lindvig et al. (2001) also showed that Eq. (12) yields poor results for solutions containing polar and hydrogen-bonding compounds. Therefore, the Hansen solubility

parameter (Hansen, 2007) should be applied instead. According to the Hansen solubility parameter theory, solubility is composed of three contributions, including non-polar forces (d), polar forces (p) and hydrogen-bonding effects (hb). That is to say, the Hildebrand solubility parameter can be expressed in terms of the dispersion part (δ_d), polar part (δ_p) and hydrogen-bonding part (δ_{hb}) (Lindvig et al., 2002):

$$\delta_i^2 = \delta_{i,d}^2 + \delta_{i,p}^2 + \delta_{i,hb}^2 \tag{13}$$

For a general solution, Lindvig et al. (2002) established a model called the Flory–Huggins/Hansen-solubility-parameter (FH/HSP) model to estimate the Flory–Huggins parameter χ_{ij}:

$$\chi_{ij} = \alpha\frac{V_{ij}}{RT}((\delta_{i,d}-\delta_{j,d})^2 + 0.25(\delta_{i,p}-\delta_{j,p})^2 + 0.25(\delta_{i,hb}-\delta_{j,hb})^2) \tag{14}$$

Hansen suggested using this expression with $\alpha=1$, particularly for a system where the dispersion forces dominate the polar and hydrogen-bonding ones (Hansen, 2007). It is worth noticing that the coefficient $\alpha=1$ is not always suitable, and for an exceptional system, α should be determined based on the database (Lindvig et al., 2002). For our water/caprolactam and benzene/caprolactam system, we use $\alpha=2$ here to derive the required Flory–Huggins parameters, as this value can produce desired interfacial tension for W/B/CPL system.

Finally, for the parameters in the surfactant model, we choose the Hansen solubility parameters of diethylene glycol (2-(2-hydroxy-ethoxy)-ethanol) and polyethylene as the counterparts of the hydrophilic head (H) group and hydrophobic tail (T) group, respectively. The Hansen solubility parameters used for different components are summarized in Table 2.

It should be noted that, although the Hansen solubility parameters in Table 2 were determined at 298 K, they change a small amount with temperature, except for the hydrogen-bonding part. Hydrogen bonding is sensitive to temperature because the hydrogen bonds are gradually broken or weakened as the temperature increases (Hansen, 2007). However, because only the difference in the hydrogen-bonding parts and not their absolute values are needed when calculating χ_{ij} (in other words, when the temperature changes slightly, the corresponding changes in $\delta_{i,hb}$ might be canceled out when applying Eq. (14)), the change in χ_{ij} is negligible. Due to this argument, the parameters at 298 K can be safely applied to the system at 293 K when calculating χ_{ij}.

Using this knowledge of χ_{ij}, the interaction parameters a_{ij} can be calculated using Eq. (4). And we choose water as the specific system to calibrate a_{ii} for all types of beads. It is worth noting that when grouping five water molecules rather than one into a DPD bead, i.e. the coarse-graining degree of water is 5 instead of 1, and correspondingly the value of a_{ii} should be 131.5 instead of 25 (Groot and Rabone, 2001). However, as explained by Maiti and McGrother (2004), a linear scaling of a_{ii} as a function of coarse-graining degree leads to an increasing surface tension deviating from experimental values, because surface tension is highly dependent on the value of the DPD interaction parameter (Goicochea et al., 2007). On the other hand, it has been reported that the choice of the interaction parameter $a_{ii}=25$ can yield desired surface tension (Maiti and McGrother, 2004; Lin et al., 2012). Therefore in present work, we adopt the latter value for a_{ii} for all beads. The final results are summarized in Table 3. All DPD beads were set to the same volume $V_{DPD}=5V_{water}=150$ Å^3, and the masses were set equal to 1.

Table 2
Hansen solubility parameters adopted in our determination of interaction parameters. These parameters were taken from Ref. Hansen (2007) at 298 K.

Molecule	δ_d (J/cm^3)$^{1/2}$	δ_p (J/cm^3)$^{1/2}$	δ_{hb} (J/cm^3)$^{1/2}$
Water	18.1	17.1	16.9
Benzene	18.4	0	2
Caprolactam	19.4	13.8	3.9
Diethylene glycol	16.6	12	20.7
Polyethylene	16	0.8	2.8

Table 3
Conservative interaction parameters a_{ij} in units of k_BT/r_c. Here W, B, and CPL represent water, benzene, and caprolactam, respectively, and H and T represent the head and tail of the surfactant, respectively.

	W	B	CPL	H	T
W	25	116.31	37.56	28.07	54.11
B	116.31	25	38.29	56.32	26.46
CPL	37.56	38.29	25	46.85	39.57
H	28.07	56.32	46.85	25	52.74
T	54.11	26.46	39.57	52.74	25

2.3. Computational details

The DPD simulation is performed using the DPD module in Materials Studio, Accelrys (2014). Usually, a finite-size effect should be carefully taken into account to properly evaluate the interfacial tension (IFT) because the calculation of the IFT is associated with the surface area of the interface (Velázquez et al., 2006; Biscay et al., 2009). In the case of the DPD simulation, the repulsive potentials are short ranged, and therefore, the simulations can be performed in a relatively small system. We set the simulation box size to $20\times10\times10\ r_c^3$ ($L_x\times L_y\times L_z$), and periodic boundary conditions are applied in all three directions. The x-direction is set to be perpendicular to the water/benzene interface. The simulation cell contains 6000 beads with a bead density of 3, and the cell is large enough for the calculation of interfacial tension (Ginzburg et al., 2011; Li et al., 2012). The other constants in the dissipative and random forces are set to $\gamma=4.5$ and $\sigma=3$ to keep the temperature fixed at $k_BT=1$. The simulation runs for 60,000 steps with a time step of 0.04. We hypothesize that this simulation time is long enough for the system to reach equilibrium. Indeed, we monitor the diffusion of each component in the simulation, and notice that these quantities become nearly constants after 2000 steps. We perform three runs for each system, and the final reported IFT is the average of three simulations.

3. Results and discussions

3.1. Water/benzene/CPL system in the absence of surfactants

3.1.1. Interfacial tension

We first validate the parameters determined above by scrutinizing the IFT of the water/benzene/CPL system. The water–benzene volume ratio is set to 1 throughout this study, and the total CPL volume fractions vary from 0 to 21.18%; this range is chosen simply to agree with the selected experimental data (van Delden et al., 2004). The interfacial tension γ_{DPD} is calculated with the difference in normal and tangential stress across the interface (Irving and Kirkwood, 1950). P is the pressure tensor, and it consists of three diagonal components P_{xx}, P_{yy}, and P_{zz}. Because the x axis is normal to the interface, the interfacial tension can be calculated using the Irving–Kirkwood equation by integrating the stress difference over x:

$$\gamma_{DPD} = \int \left[P_{xx} - \frac{1}{2}(P_{yy}+P_{zz})\right] dx \tag{15}$$

To compare our simulation predictions directly with the experimental data, we need to convert the interfacial tension from

DPD units, r_c^2/k_BT, to conventional units (mN/m) (Groot and Rabone, 2001; Scocchi et al., 2007). Because the volume of one bead is 150 Å^3 and the number density is $\rho r_c^3 = 3$, a cube corresponds to a volume of 450 Å^3. Thus, the cut-off radius in conventional unit can be obtained:

$$r_c = \sqrt[3]{450}\ \text{Å} = 7.66\ \text{Å} \tag{16}$$

Therefore, the interfacial tension scale can be calculated as

$$k_BT/r_c^2 = 1.38 \times 10^{-23} \times 293/(7.66 \times 10^{-10})^2\ N/m = 6.889\ \text{mN}/m. \tag{17}$$

Thus, the correspondence between the conventional and simulated interfacial tensions can be converted via

$$\gamma = (k_BT/r_c^2)\gamma_{DPD} \tag{18}$$

Using Eq. (18), we can obtain the DPD results for the interfacial tension in units of mN/m for the water/benzene interface with different volume fractions of CPL in the water-rich phase. Because the density of CPL is very close to that of water, the volume fraction in the water-rich phase is nearly equivalent to its mass fraction, which is usually determined in experiments. In addition, because of the relative low solubility of CPL in the benzene-rich phase, we assume that the total CPL volume fractions in both phases can be approximately determined from the mass fractions of CPL in the water-rich phase.

The experimental data are extracted for comparison with the DPD simulation results, and this comparison is shown in Fig. 2. The experimental data are taken from van Delden et al. (2004) (with CPL) and from Alpbaz et al. (1988) (without CPL). Compared with the experimental results, our simulated interfacial tension is satisfactory. In particular, when the weight percentage of CPL in the water-rich phase is larger than 5%, the simulated descending line is almost parallel to the experimental line, which means that the descending gradient of the DPD results is nearly the same as that of the experimental data. However, the experimental interfacial tension between the water/benzene interface apparently drops faster than the DPD prediction at low weight percentages of CPL. For further comparison, we also plot the SCFT results from Tuinier and Krooshof (2012) at a slightly different temperature, and similar trend is observed when a comparison is made between the SCFT results and the experimental data. One possible reason for this trend is that the experiment involves a very small amount of impurities containing the surface-active ingredients, which commonly reduce the interfacial tension. The similarity between our predicted results and SCFT and the experimental data justifies our coarse-grained model.

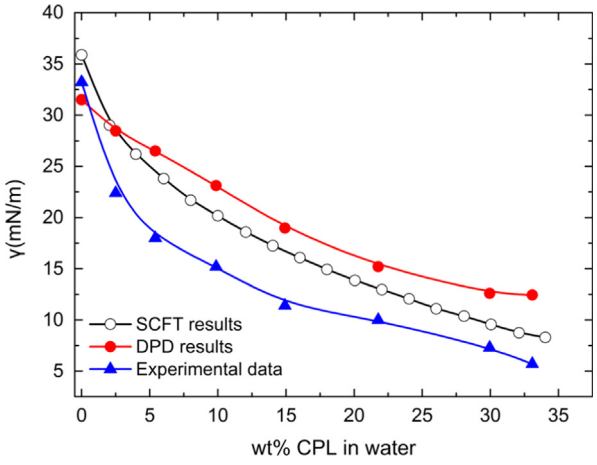

Fig. 2. The interfacial tension of the water/benzene interface as a function of the CPL wt% in the water-rich phase in comparison with experimental data (van Delden et al., 2004; Alpbaz et al., 1988) and SCFT data (Tuinier and Krooshof, 2012). The curves are drawn to guide the eye.

3.1.2. Density profiles near the interface

To analyze the equilibrium behavior of CPL in the water/benzene system, the density profiles of W/B/CPL systems with different volume fractions of CPL are calculated and shown in Fig. 3. We choose the four most characteristic systems from our database for investigation, i.e., the volume fractions of CPL equal to 0, 2.96%, 8.6%, and 13.06%. As seen in Fig. 3, as the volume fraction of CPL increases, its number density increases significantly at the interface, which means the CPL molecules tend to remain at the interface rather than dissolve into the water-rich phase or the benzene-rich phase. This behavior indicates that CPL acts like a (weak) surfactant in the water/benzene system, which is confirmed by checking the interaction parameters in Table 3, i.e., the interaction parameter a_{ij} of CPL with benzene or water is similar to, but stronger than, that of a surfactant. Moreover, we also find that the density gradient within the interfacial zone becomes less sharp when the volume fraction of CPL increases, which illustrates that the presence of CPL screens the strong repulsion between water and benzene at the interface. The surface activity of CPL might be driven by the weak repulsion from water and the slightly stronger repulsion from benzene, while due to the small difference between the water-CPL interaction parameter ($a_{ij} =$ 37.56) and the benzene-CPL interaction parameter ($a_{ij} = 38.29$), the CPL beads are not inclined to penetrate into either the water-rich phase or the benzene-rich phase; instead, they cluster together and remain at the water/benzene interface.

Comparing Figs. 2 and 3, one can find that CPL accumulates at the interface and decreases the interfacial tension of the water/benzene interface. In general, the adsorption of CPL beads at the interface relaxes the unfavorable interaction between water and benzene and, therefore, CPL acts like a weak surfactant.

3.2. Water/benzene/CPL system with the addition of surfactants

3.2.1. Influence of the surfactant tail length

The surfactant tail length has a direct influence on the interfacial tension, which can be explained using Traube's rule for simple interfacial systems when the surfactants are considered (Rekvig et al., 2003; Smit, 1988; Smit et al., 1990). Traube's rule states that longer hydrophobic tail lengths have greater surface activity than short chain lengths. However, the presence of CPL in the water/benzene system may have an interesting influence; thus, the effect of the surfactant tail length on the water/benzene interface is worth investigating.

We consider four types of surfactants with different chain lengths: HT, HT_3, HT_5, and HT_7. In these systems, the volume fraction of CPL is fixed at 5%, and as before, the water/benzene volume ratio is equal to 1. We borrow the term *efficiency at the interface* to describe the influence of the surfactant tail length on the interfacial properties. The *efficiency at the interface* of the surfactants was first proposed by Rekvig et al. (2003), and it is defined as the number of surfactants required to obtain the corresponding interface effect. We define the surfactant density at the interface as the number of surfactants adsorbed at the interface divided by twice the cross-sectional area of the simulation box. If the same interfacial tension is achieved with a lower surfactant density, then the efficiency of the surfactant is higher. Equivalently, given the same surfactant density, the one with the lower interfacial tension has a higher efficiency.

Fig. 4 shows the normalized interfacial tension versus the surfactant density at the water/benzene interface for four different

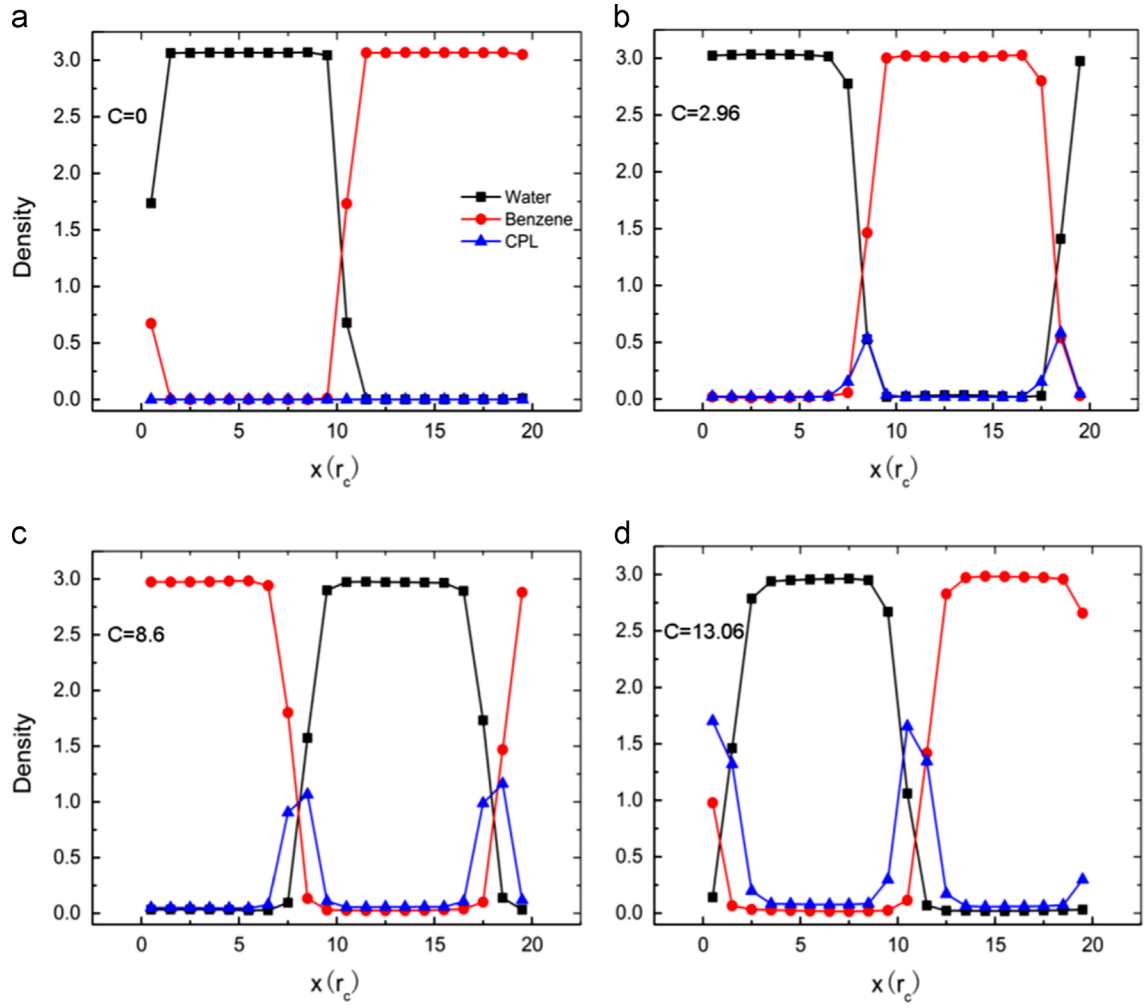

Fig. 3. Density profiles for water beads (black squares), benzene beads (red circles) and CPL beads (blue triangles). (a) The volume fractions of CPL are equal to 0; (b) volume fractions of CPL are equal to 2.96%; (c) volume fractions of CPL are equal to 8.6%; and (d) volume fractions of CPL are equal to 13.06%. The curves are drawn to guide the eye. (For interpretation of the references to color in this figure legend, the reader is referred to the web version of this article.)

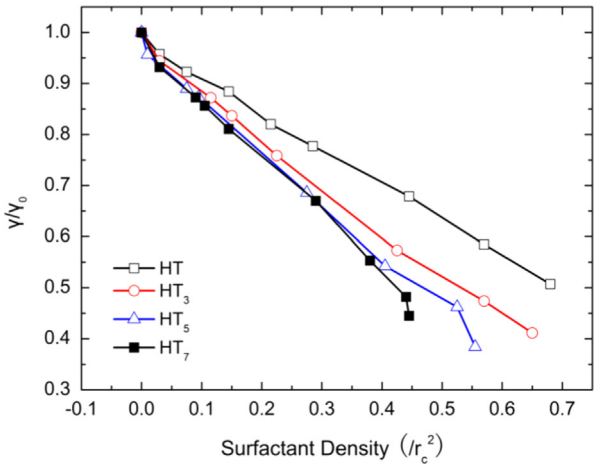

Fig. 4. Normalized interfacial tensions versus the surfactant density at the interface. The curves are drawn to guide the eye.

types of surfactants. The normalized interfacial tension is introduced by dividing by the interfacial tension for the W/B/CPL system without surfactant, γ_0. When the surfactant density is low, the averaged distance between the surfactants is large, and the interactions between them are relatively small. In this case, the interfacial efficiencies for the four types of surfactants are almost the same, as shown in Fig. 4. When the surfactant density increases, the surfactants with longer hydrophobic tails display higher efficiencies at the interface. This trend generally agrees with Traube's rule.

However, we can see that when the tail length of the surfactant is short (i.e., $m \leq 3$), increasing the tail length generates significant increases in the efficiency of the surfactant. When the tail length of the surfactant is long, the increase is negligible, especially at low surfactant densities, which is different from the situation in the absence of CPL (Rekvig et al., 2003). For instance, the line for HT_5 in Fig. 4 almost overlaps HT_7 when the surfactant density range is from 0 to 0.3. It seems that this result deviates from the conventional phenomenon complying with Traube's rule. And situation for HT_5 seems a critical point for this deviation. So, to illustrate the exception, we plot the normalized interfacial tensions versus surfactants density for HT_3, HT_5 and HT_7 with or without the presence of CPL in Fig. 5(a). The data of curves with CPL are directly taken from Fig. 4. The curves without CPL are calculated with our own DPD interaction parameters under the conditions mentioned in Section 2.3. It should be noted that, for systems without CPL, increasing the tail length enhances the interfacial efficiency of a surfactant, which is in agreement with Traube's rule. And we can also qualitatively see the difference, i.e., the normalized interfacial tensions with CPL decreases faster than that without CPL.

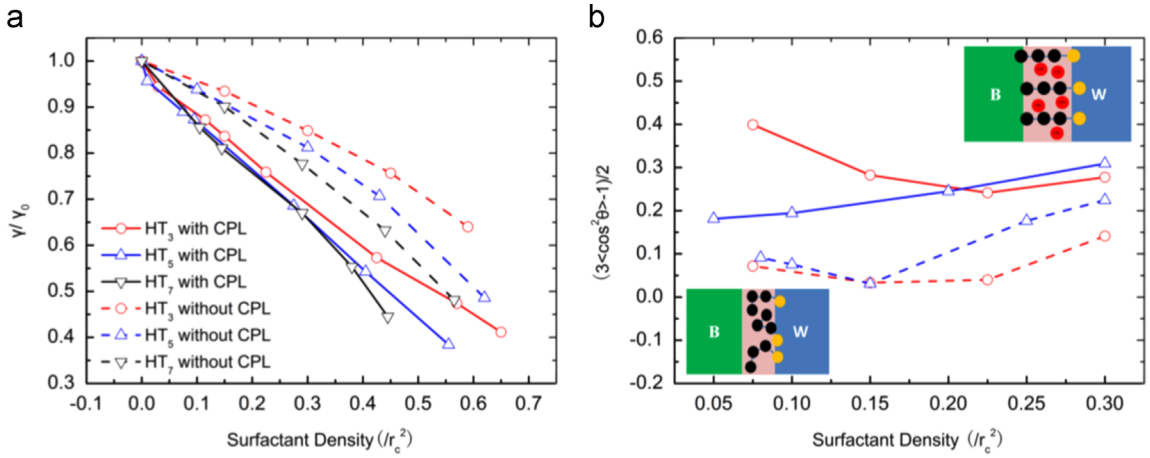

Fig. 5. (a) Normalized interfacial tensions versus surfactants density for HT_3, HT_5 and HT_7 with (solid line) and without (dashed line) CPL. (b) Comparisons of order parameters of surfactants at the interface with (solid lines) or without (dashed lines) CPL. See text for details.

To understand the exception, we first study the conformational information of surfactants at the interface with and without the presence of CPL. In Fig. 5(b), we plot the order parameter $(3\langle\cos^2\theta\rangle-1)/2$ varying with surfactant density. Here θ is the angle between the bond connecting the head group and first bead in the tail group and the normal vector of the interface. The order parameter demonstrates the degree of alignment of surfactants at the interface at different surfactant densities. When the order parameter is larger, the averaged alignment of surfactants is more perpendicular to the interface, and vice versa. The solid lines represent the order parameters for the systems with CPL, and the dashed lines for those without CPL. The curves with circles represent HT_3, and the ones with triangles for HT_5. Fig. 5 (b) demonstrates the comparison of order parameters between both systems in the absence or presence of CPL at various surfactant tail lengths. The comparisons show that the presence of CPL drives the surfactants more perpendicular to the interface. It should be noted that, because different tail lengths impose different influences on the calculation of order parameter, it is less meaningful to compare the order parameters between the systems with different surfactants.

Besides, we need to consider the resultant influence of the association of surfactants at the interface to the interfacial thickness in detail. The interfacial thickness is conventionally defined as the length along the interface normal direction over which the density of one major component ranges from 10% to 90% of their bulk value (Luo and Dai, 2007). The interfacial thickness versus the tail length is plotted in Fig. 6. Here the surfactant density at the interface is fixed at 0.3. We also check the density distributions of CPL and the surfactant tail in the presence of four types of surfactants. The surfactant density and volume fractions of CPL in the four systems are kept the same (0.3 and 5%, respectively). The density profiles of CPL and the surfactant tails are plotted in Fig. 7, which shows that the density distributions of CPL are almost the same and that CPL remains at the interface in the four systems as a weak surfactant. In Fig. 7, we also plot the density profile of the surfactant tail. This figure shows that when the surfactant tail length increases, the peak of its density distribution is closer to the benzene-rich phase, which indicates, in combination with Fig. 6, that when the surfactant tail length becomes longer, the surfactant molecules are more likely located along the x axis, i.e., perpendicular to the interface, as shown in the upper panel of Fig. 5(b). To further illustrate the relationship between tail beads and CPL while tail length increases, additionally, radial distribution functions (RDF) between tails beads and CPL are shown in Fig. 8 for different types of surfactants with the same surfactant density and

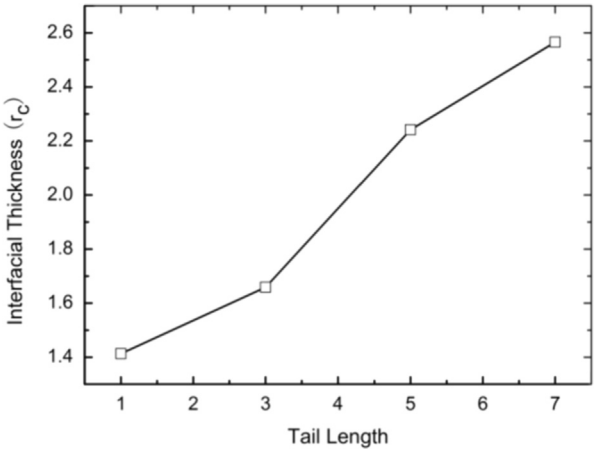

Fig. 6. The interfacial thicknesses versus tail length with a surfactant density at the interface of 0.3. Volume fraction of CPL is fixed at 5%. The curves are drawn to guide the eye.

volume fraction of CPL. The RDF is defined as

$$g(r)=\frac{n(r)}{(4\pi/3)[(r+dr)^3-r^3]\rho^0} \tag{19}$$

where $n(r)$ is the number of CPL beads at a distance between r and $r+dr$ from each tail bead; and ρ^0 is the number density of CPL particles in the entire simulation box.

Now, we discuss the effect of the tail length on the efficiency of the surfactant in the presence of CPL. For convenience, we use the concept "repulsion energy density". The repulsion energy density refers to the repulsion energy per volume at the interface, which is closely related to the degree of saturation. A unit volume contains more repulsively interacting beads, and then the repulsion energy density is higher, and apparently the degree of saturation is higher. For the water/benzene/CPL system with surfactant, the repulsion at the interface mainly comes from CPL-CPL, CPL-surfactant, and surfactant–surfactant repulsions. The maximum value of this repulsion energy density at the interface should be associated with the interaction of the CPL/surfactant with water/benzene. If the repulsion energy density exceeds its maximum value, some component, e.g., CPL, as shown below, will be driven into the bulk phase to reduce the repulsion energy density at the interface.

When the surfactant has a short tail length (i.e., $m\leq 3$), increasing the surfactant tail length is equivalent to increasing the number density of hydrophobic beads, which tends to increase

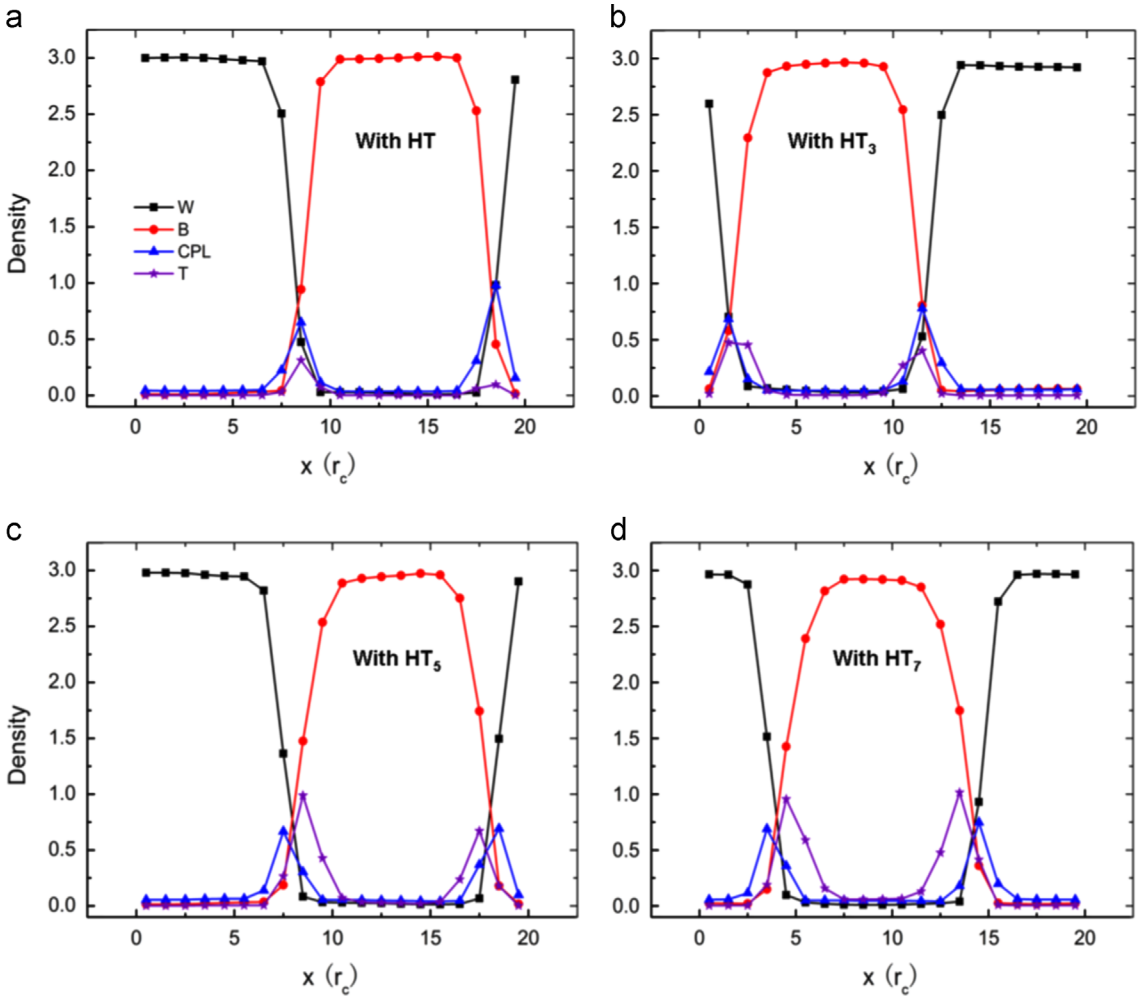

Fig. 7. Density profiles of water (black line with squares), benzene (red line with circles), CPL (blue line with triangles), and surfactant tail (purple line with stars) at the interface in the presences of four types of surfactants. The surfactant density and the volume fraction of CPL in the four systems are kept the same (0.3 and 5%, respectively). (For interpretation of the references to color in this figure legend, the reader is referred to the web version of this article.)

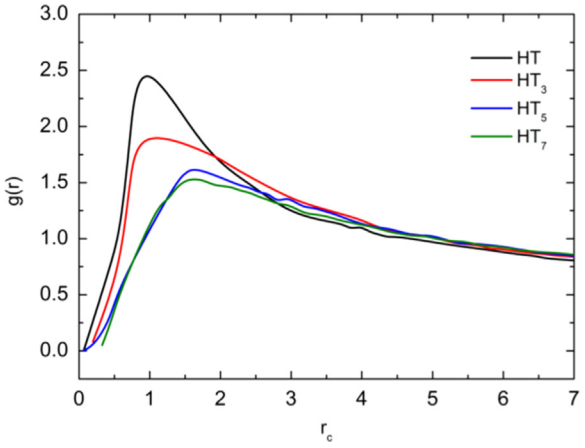

Fig. 8. Radial distribution functions (RDF) of HT (black line), HT_3 (red line), HT_5 (blue line), and HT_7 (green line) between their tail beads and CPL. The surfactant density and the volume fraction of CPL in the four systems are kept the same (0.3 and 5%, respectively). (For interpretation of the references to color in this figure legend, the reader is referred to the web version of this article.)

the repulsion between the surfactants and the CPLs because they locate at the same place in the interface zone (see Fig. 7(a) and (b)), which leads to a higher lateral pressure (Rekvig et al., 2003), i.e., P_{yy} and P_{zz} become larger. From Eq. (15), it is clear that this feature reduces the interfacial tension or, equivalently, improves the surfactant efficiency. Moreover, given that CPL behaves like surfactant, its presence at the interface in some sense increases the surfactant density, which explains why the normalized interfacial tension with CPL reduces faster than without CPL when increasing the surfactant density, as shown in Fig. 5(a). However, owing to surfactants' stronger tendency to remain at the interface, further increasing the surfactant density will drive the CPL molecules into the bulk phase otherwise the repulsion energy density at the interface becomes too high, and in this case, the presence of CPL in the system becomes irrelevant to the surfactant efficiency.

When the tail length of the surfactant increases, the number density of hydrophobic surfactant tail beads doubles or triples or increases by an even greater rate with the same surfactant density at the interface compared with surfactants with short tail length. In this case, when CPL and surfactants are simultaneously present, the interface saturates more rapidly because CPL acts as a weak surfactant, especially at low surfactant densities. And as shown in Fig. 7(c) and (d), the density distribution of the surfactant tail beads gradually moves away from CPL. The same phenomenon can been clearly observed in Fig. 8 as well, the apex in RDF of surfactants with longer tail is smaller in value $g(r)$ but larger in value r when compared with the one in RDF of surfactants with short tail length. That is to say, tail beads in the long tail are farther from CPL beads than those in the short tail. This phenomenon is probably because the tail bead-CPL repulsion is stronger than the

tail bead–benzene repulsion; thus, the surfactant is likely to fully extend in the interface to reduce the strong repulsion from CPL, which is indicated by Figs. 5(b) and 6. In other words, if we further increase the surfactant tail length, the repulsion between CPL and surfactant will not increase significantly, and then it becomes increasingly difficult to further reduce the interfacial tension, which is equivalent to saying that the tail length effect on the surfactant efficiency is negligible. However, if we fix the tail length and increase the surfactant density, the repulsion among surfactants still increases due to the stronger tendency of surfactants to remain at the interface. As a result, the interfacial tension continues to decrease, as shown in Fig. 4. In contrast, if there is no CPL in the system, the tail bead–bead repulsion is weaker than tail bead–benzene repulsion, and thus, the surfactant is likely to curl over in the interfacial zone to reduce the repulsion from the benzene phase (see the bottom panel in Fig. 5(b)), which increases the repulsion between surfactants; thus, the tail length effect on the surfactant efficiency is in agreement with Traube's rule (see dashed line in Fig. 5(a)).

3.2.2. Effect of CPL on surfactant efficiency

In the above calculations, the CPL volume fraction is fixed at 5%. To further understand the effect of CPL on the surfactant efficiency, we check the normalized interfacial tension using four different CPL volume fractions, i.e., 0, 3%, 5% and 7%. In this case, the surfactant tail length is fixed. Fig. 9 shows the influence of CPL on the interfacial efficiency of the surfactant HT_5. The curves are drawn to illustrate the normalized interfacial tension versus surfactant density of HT_5 at the interface. The four curves correspond to the four systems with different CPL volume fractions as indicated in the figure, and the interfacial tension without HT_5, i.e., γ_0, is separately calculated for each system with CPL at the corresponding volume fraction.

As shown in Fig. 9, the increase in the volume fraction of CPL apparently enhances the interfacial efficiency of HT_5. As more CPL is added, stronger activation is achieved. Based on the above argument, this result is because CPL accumulates at the interface as a weak surfactant, and the increase in its volume fraction subsequently leads to a higher repulsion at the interface because the interfacial thickness is less sensitive to the volume fraction of CPL. The interfacial thickness in terms of the volume fraction of CPL is depicted in Fig. 10 at three fixed surfactant densities of 0.1, 0.3 and 0.45. As expected, the increase of interfacial thickness is overall small with respect to the increase of CPL volume fraction, especially when the surfactant density is low. When the surfactant density is higher, the increase of interfacial thickness is more

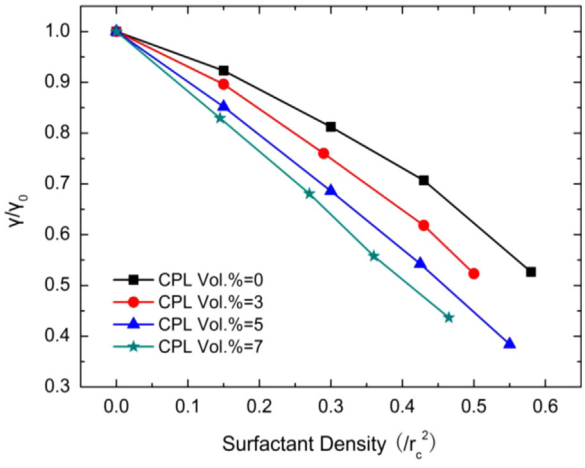

Fig. 9. Normalized interfacial tension versus surfactant density for HT_5 at different vol% of CPL. The curves are drawn to guide the eye.

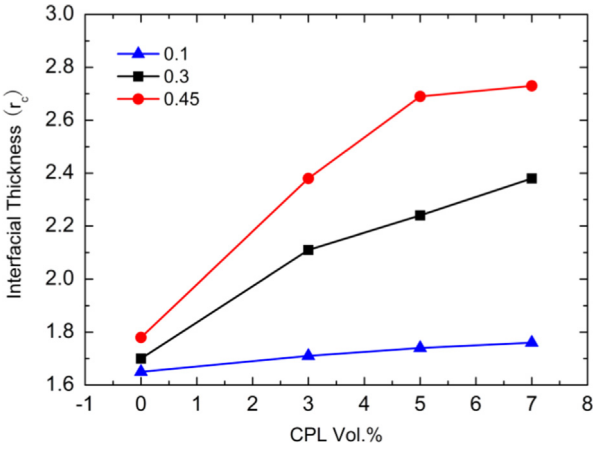

Fig. 10. The interfacial thickness versus the volume fraction of CPL with three fixed surfactant densities of 0.1 (blue triangles), 0.3 (black squares) and 0.45 (red circles) for surfactant HT_5. The curve is drawn to guide the eye. (For interpretation of the references to color in this figure legend, the reader is referred to the web version of this article.)

significant, and this effect is consistent with the curves in Fig. 9, i.e., at a given higher surfactant density the increase of CPL volume fraction leads to a more significant change of the normalized interfacial tension. Besides, Fig. 10 confirms that at given CPL volume fraction, the increase of surfactant density leads to an apparent increase of interfacial thickness.

3.2.3. Influence of surfactant concentration

As the surfactant concentration increases, the surfactants create diverse and complex structures. The self-aggregation behaviors of pure, non-ionic surfactants have been theoretically investigated by Ryjkina et al. (2002). Increasing the concentration of non-ionic surfactants in the water/benzene/CPL system has an interesting impact on the distribution of CPL, as shown in Fig. 11. Fig. 11 shows snapshots of the DPD simulations for four systems with different surfactant concentrations, and the corresponding density distributions of CPL (on the right) are also plotted next to the snapshots (on the left). In these four systems, the CPL volume fractions are fixed at 5% and the water/benzene volume ratio is set to 1. The CPL density distribution profiles are collected along the x axis.

Compairing Fig. 11(a) and (e), we can see that, when the surfactants density is low (e.g., volume fraction is 16%), the surfactants are inclined to remain at the interface and form a lamellar structure. When the surfactants density exceeds a critical value, as shown in Fig. 11(c) and (g), a rod structure of the water-rich phase is formed and surrounded by surfactants with their heads penetrating into the water phase. This phenomena is similar to the aggregation of surfactants in the bulk system (Ryjkina et al., 2002). The formation of rod structures might be due to the strong tendency of the head groups to enter the water phase. A rod structure rather than a rectangular one can provide a larger surface area for the surfactants to interact with. However, in principle, a spherical structure should be observed in such emulsion-like system. The absence of a spherical structure is caused by the finite-size effects of the simulation system because the spherical structure is comparable to the size of box when the simulation box is small. To validate this hypothesis, we perform a simulation with a larger box size of $30 \times 30 \times 30 r_c^3 (L_x \times L_y \times L_z)$, and when the volume fraction of HT_3 is set to 32%, a spherical structure is observed, which is shown in Fig. 12. In Fig. 12(a), we show the isopycnic surface of the head groups. Because the water-rich phase is surrounded by head groups, the isopycnic surface of the head groups can reflect the morphology of the water-rich

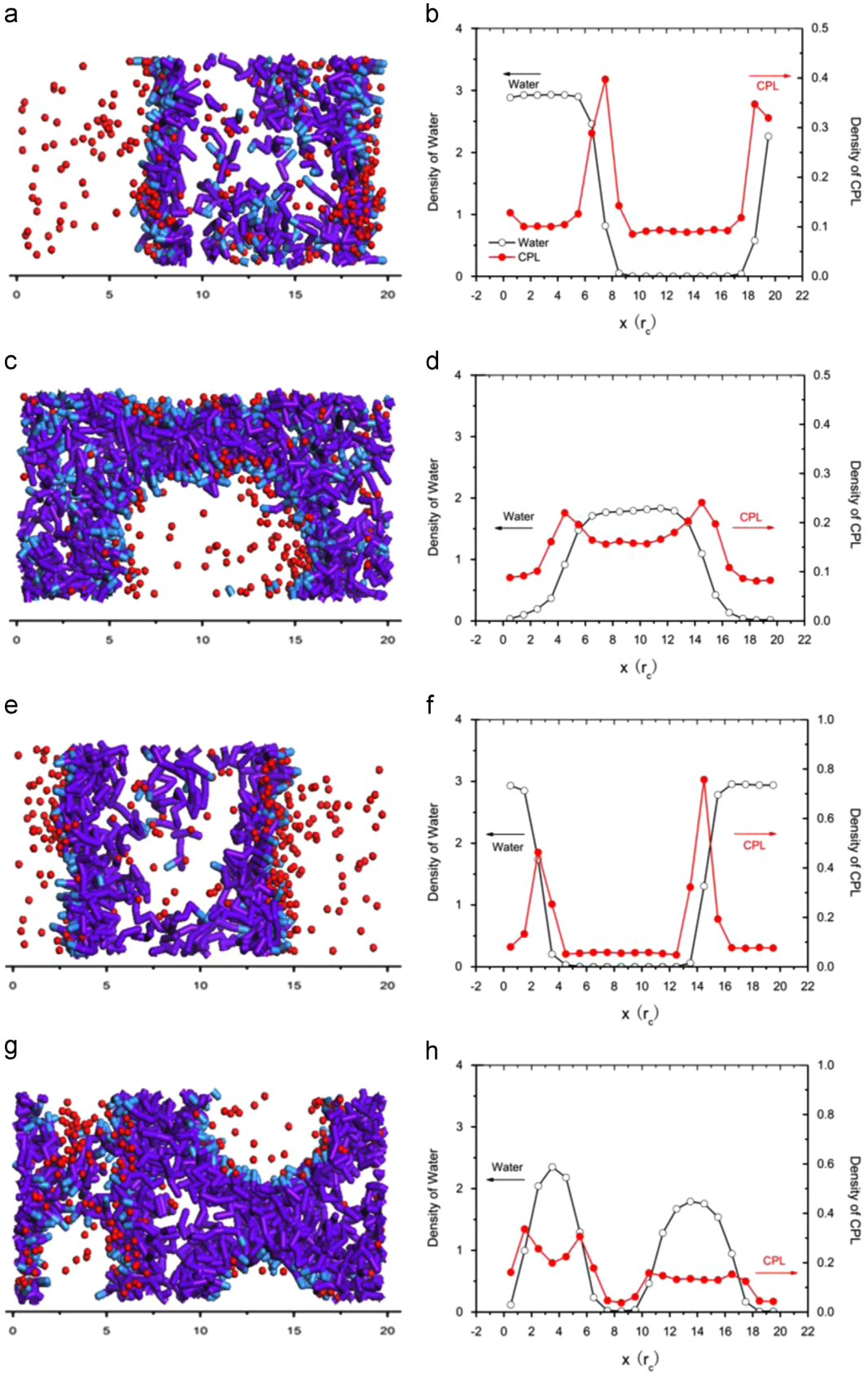

Fig. 11. Snapshots of the four W/B/CPL/surfactants systems with different surfactant concentrations or different surfactant tail lengths (on the left) and the corresponding density profile of the water and CPL along the *x* axis (on the right). From top to bottom, the surfactant is (a and b) HT_3 with 16% volume fraction, (c and d) HT_3 with 32% volume fraction, (e and f) HT_7 with 16% volume fraction, and (g and h) HT_7 with volume fraction 32%. For simplicity, the water beads and benzene beads are not shown in the snapshots. The surfactant head groups are in blue, the tail groups in violet, and the CPL beads in red. (For interpretation of the references to color in this figure legend, the reader is referred to the web version of this article.)

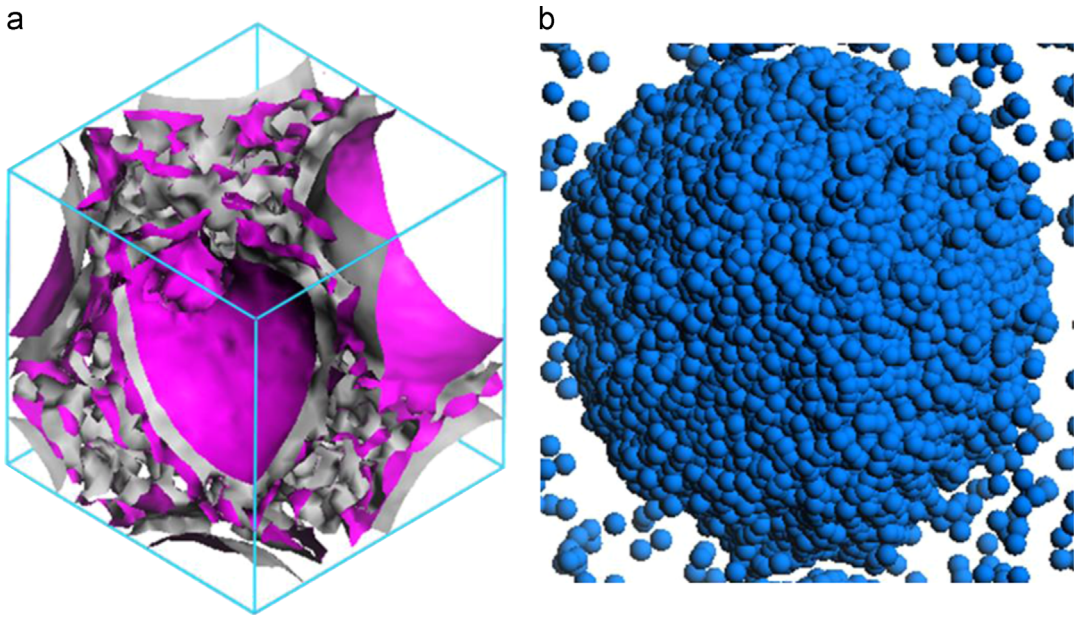

Fig. 12. Snapshots of a larger simulation system when the volume fraction of HT_3 is set to 32%. (a) The isopycnic surface of the surfactant head groups and (b) structure of the water-rich phase; for simplicity, only the water beads are shown. See the text for details.

phase. When we extend the simulation box using periodic boundary condition, we observe a complete spherical structure for the water-rich phase, which is displayed in Fig. 12(b). This observed structure is similar to a w/o-type droplet in nano-emulsion. The diameter of this droplet from our simulation is approximately 20 nm (or equivalently $25r_c$), which is in consistence with the reported experimental data (15–120 nm) (Porras et al., 2004), although the composition of emulsions varies a little in simulation and experiments.

Regarding the distributions of CPL in the system with different water phase morphologies, we confirm that when the surfactant volume fraction is low, CPL still tends to remain at the interface, as shown in Fig. 11(b) and (f). By comparing Fig. 3 (without surfactant) and Fig. 7 (surfactant density at the interface is 0.3), we can see that the number densities of CPL in the water-rich phase and in the benzene-rich phase become finite but are almost the same, which means that further addition of the surfactant (with a fixed tail length) drives the CPL away from the interface. If the surfactant volume fraction is high, it appears that the number density of CPL in the water-rich phase becomes significantly larger than that in the benzene-rich phase, as shown in Fig. 11(d) and (h).

The interpretation of this interesting phenomenon can be obtained by comparing the interaction parameters in Table 3. As we explained above, CPL behaves like weak surfactant. When a real surfactant is introduced, the surfactant molecules preferably remain at the interface and exert repulsive forces on CPL. As indicated in Table 3, CPL preferably interacts with water over benzene, which is why the addition of a certain amount of surfactant drives CPL from the interface and into the both water and benzene phases. As more surfactants are introduced, more CPL molecules are driven away, which determines the solubility of CPL in benzene and water. Due to the higher solubility of CPL in water, more CPL molecules migrate into the water-rich phase. This mechanism can be applied to an industrial CPL extraction process and to improve the extraction efficiency. Moreover, because the addition of surfactants with long tails also increases the interfacial thickness, resulting in more CPL molecules in the interfacial zone, surfactants with short tails are preferably employed for higher extraction efficiency.

4. Conclusions

In this study, we employ a dissipative particle dynamics method to investigate the water/benzene/CPL system in the presence of surfactants. The system is described using a coarse-grained model and the involved interaction parameters are derived by combining the Hildebrand-solubility-parameters model and the Flory–Huggins/Hansen-solubility-parameter (FH/HSP) model. We first validate our interaction parameters by comparing the DPD simulation prediction of the interfacial tension for the water/benzene/CPL system with the results from experiments and SCFT. The comparison shows that the predicted interfacial tensions at various CPL mass fractions are quantitatively good but with an upward shift when the CPL density is large. This satisfactory comparison shows that the coarse-grained model we developed is reasonable and capable of describing the interface system.

After the interaction parameters are rationalized, we further study the water/benzene/CPL system in the presence of various surfactants. Specifically, we investigate the surfactant efficiency at different surfactant tail lengths and different volume fractions of CPL, and find that if the tail length of the surfactant is small, increasing the tail length increases the efficiency of the surfactant; this trend generally obeys Traube's rule. If the tail length exceeds a critical value, due to the presence of CPL at the interface, the tail length effect on the efficiency of the surfactant is almost negligible, which is different from the tail length effect in the water/benzene system wherein increasing the CPL density always enhances the efficiency of surfactant. We also determine the density distribution of CPL as the surfactant concentration increases. We show that, at low surfactant concentrations, CPL accumulates at the interfacial zone, and at high surfactant concentrations, CPL molecules are forced away from the interfacial zone and move into the water-rich phase.

The results of our study provide helpful understandings on the microscopic behavior of surfactants at water/benzene interface in the presence of CPL. The new insight we gained is that CPL, like a weak surfactant, is capable of activating surfactants at the interface by improving the efficiency of the surfactant. The addition of surfactants with short tail lengths into the water/benzene/CPL

system can drive CPL into the water-rich phase, and this mechanism could be applied to the design of more efficient industrial extraction process. We expect for experimental data to verify our prediction.

Finally, current study on CPL extraction is based on equilibrium simulations. However, in industrial extraction, dynamical processes, e.g., CPL transporting in shear flow, may bring profound effects on the extraction efficiency. Towards those effects, simulations addressing the dynamic properties can provide further insight into the extraction process of CPL, which, however, is out of research scope of present work and will be considered in our future work.

Acknowledgments

This work is supported by the National Basic Research Program of China (2014CB748500), the National Natural Science Foundation of China (No. 91334203), the 111 Project of Ministry of Education of China (National Natural Science Foundation of China No. B08021) and the Fundamental Research Funds for the Central Universities. SZ acknowledges the support of Shanghai Science and Technology Committee Rising-Star Program (Grant no. 14QA1401300). The authors also thank Professor Charles M. Hansen and Professor Georgios Kontogeorgis for their helpful suggestions.

References

Alpbaz, M., Bilgesü, A., Tutkun, O., 1988. Measurement of interfacial tension by drop method. Commun. Fac. Sci. Univ. Ank. Ser. B 34, 103–112.
Aswal, V.K., Goyal, P.S., Kohlbrecher, J., Bahadur, P., 2001. SANS study of salt induced micellization in PEO–PPO–PEO block copolymers. Chem. Phys. Lett. 349 (5–6), 458–462.
Barton, A.F.M., 1975. Solubility parameters. Chem. Rev. 75 (6), 731–753.
Biscay, F., Ghoufi, A., Goujon, F., Lachet, V., Malfreyt, P., 2009. Calculation of the surface tension from Monte Carlo simulations: does the model impact on the finite-size effects? J. Chem. Phys. 130 (18), 184710.
Dsinter-De Hondt, M.L.C., Lemmens, J.A.W., 2004. Process for recovering and purifying caprolactam from an organic solvent. US20040110943, A1.
Emborsky, C.P., Cox, K.R., Chapman, W.G., 2011. Exploring parameter space effects on structure–property relationships of surfactants at liquid–liquid interfaces. J. Chem. Phys. 135 (8), 084708.
Español, P., Warren, P., 1995. Statistical mechanics of dissipative particle dynamics. Europhys. Lett. 30 (4), 191–196.
Ginzburg, V.V., Chang, K., Jog, P.K., Argenton, A.B., Rakesh, L., 2011. Modeling the interfacial tension in oil–water-nonionic surfactant mixtures using dissipative particle dynamics and self-consistent field theory. J. Phys. Chem. B 115 (16), 4654–4661.
Goicochea, A.G., Romero-Bastida, M., López-Rendón, R., 2007. Dependence of thermodynamic properties of model systems on some dissipative particle dynamics parameters. Mol. Phys. 105 (17–18), 2375–2381.
Groot, R.D., Rabone, K.L., 2001. Mesoscopic simulation of cell membrane damage, morphology change and rupture by nonionic surfactants. Biophys. J. 81 (2), 725–736.
Groot, R.D., Warren, P.B., 1997. Dissipative particle dynamics: bridging the gap between atomistic and mesoscopic simulation. J. Chem. Phys. 107 (11), 4423.
Hansen, Charles M., 2007. Hansen Solubility Parameters: A User's Handbook. CRC Press, Boca Raton, FL p. 519.
Hildebrand, J.H., Wood, S.E., 1933. The derivation of equations for regular solutions. J. Chem. Phys. 1 (12), 817.
Hoogerbrugge, P.J., Koelman, J.M.V.A., 1992. Simulating microscopic hydrodynamic phenomena with dissipative particle dynamics. Europhys. Lett. 19 (3), 155–160.
Irving, J.H., Kirkwood, J.G., 1950. The statistical mechanical theory of transport processes. IV. The equations of hydrodynamics. J. Chem. Phys. 18 (6), 817.
Larson, R.G., 1992. Monte Carlo simulation of microstructural transitions in surfactant systems. J. Chem. Phys. 96 (11), 7904.
Li, Y., Guo, Y., Bao, M., Gao, X., 2011. Investigation of interfacial and structural properties of CTAB at the oil/water interface using dissipative particle dynamics simulations. J. Colloid Interface Sci. 361 (2), 573–580.
Li, Y., Guo, Y., Xu, G., Wang, Z., Bao, M., Sun, N., 2012. Dissipative particle dynamics simulation on the properties of the oil/water/surfactant system in the absence and presence of polymer. Mol. Simul. 39 (4), 1–10.
Lin, S., Xu, M., Yang, Z., 2012. Dissipative particle dynamics study on the mesostructures of n-octadecane/water emulsion with alternating styrene–maleic acid copolymers as emulsifier. Soft Matter 8 (2), 375–384.
Lin, Y., Skaff, H., Emrick, T., Dinsmore, A.D., Russell, T.P., 2003. Nanoparticle assembly and transport at liquid-liquid interfaces. Science 299 (5604), 226–229.
Lindvig, T., Michelsen, M.L., Kontogeorgis, G.M., 2001. Thermodynamics of paint-related systems with engineering models. AIChE J. 47 (11), 2573–2584.
Lindvig, T., Michelsen, M.L., Kontogeorgis, G.M., 2002. A Flory–Huggins model based on the Hansen solubility parameters. Fluid Phase Equilib. 203, 247–260.
Lu, J.R., Thomas, R.K., Penfold, J., 2000. Surfactant layers at the air/water interface: structure and composition. Adv. Colloid Interface Sci. 84, 143–304.
Luo, M., Dai, L.L., 2007. Molecular dynamics simulations of surfactant and nanoparticle self-assembly at liquid–liquid interfaces. J. Phys. Condens. Matter 19 (37), 375109.
Luu, X.-C., Yu, J., Striolo, A., 2013. Ellipsoidal Janus nanoparticles adsorbed at the water–oil interface: some evidence of emergent behavior. J. Phys. Chem. B 117 (44), 13922–13929.
Maiti, A., McGrother, S., 2004. Bead-bead interaction parameters in dissipative particle dynamics: relation to bead-size, solubility parameter, and surface tension. J. Chem. Phys. 120 (3), 1594–1601.
Marshall, B.D., Cox, K.R., Chapman, W.G., 2012. A classical density functional theory study of the neat n-alkane/water interface. J. Phys. Chem. C 116 (33), 17641–17649.
Materials Studio, Accelrys©, 2001–2014. Accelrys Software Inc.
Mayoral, E., Goicochea, A.G., 2013. Modeling the temperature dependent interfacial tension between organic solvents and water using dissipative particle dynamics. J. Chem. Phys. 138 (9), 094703.
Porras, M., Solans, C., González, C., Martínez, A., Guinart, A., Gutiérrez, J.M., 2004. Studies of formation of W/O nano-emulsions. Colloids Surf. A Physicochem. Eng. Asp. 249, 115–118.
Rekvig, L., Kranenburg, M., Vreede, J., Hafskjold, B., Smit, B., 2003. Investigation of surfactant efficiency using dissipative particle dynamics. Langmuir 19 (20), 8195–8205.
Richtering, W., Laeuger, J., Linemann, R., 1994. Shear orientation of a micellar hexagonal liquid crystalline phase: a rheo and small angle light scattering study. Langmuir 10 (11), 4374–4379.
Ryjkina, E., Kuhn, H., Rehage, H., Müller, F., Peggau, J., 2002. Molecular dynamic computer simulations of phase behavior of non-ionic surfactants. Angew. Chem. Int. Ed. Engl. 41 (6), 983–986.
Scatchard, G., 1931. Equilibria in non-electrolyte solutions in relation to the vapor pressures and densities of the components. Chem. Rev. 8 (2), 321–333.
Schlossman, M.L., Tikhonov, A.M., 2008. Molecular ordering and phase behavior of surfactants at water–oil interfaces as probed by x-ray surface scattering. Annu. Rev. Phys. Chem. 59, 153–177.
Scocchi, G., Posocco, P., Fermeglia, M., Pricl, S., 2007. Polymer–clay nanocomposites: a multiscale molecular modeling approach. J. Phys. Chem. B 111 (9), 2143–2151.
Smit, B., 1988. Molecular-dynamics simulations of amphiphilic molecules at a liquid–liquid interface. Phys. Rev. A 37 (9), 3431–3433.
Smit, B., Schlijper, A.G., Rupert, L.A.M., Van Os, N.M., 1990. Effects of chain length of surfactants on the interfacial tension: molecular dynamics simulations and experiments. J. Phys. Chem. 94 (18), 6933–6935.
Sun, H., 1998. COMPASS: an ab initio force-field optimized for condensed-phase applications overview with details on alkane and benzene compounds. J. Phys. Chem. B 102 (38), 7338–7364.
Tuinier, R., Krooshof, G.J.P., 2012. Interfacial tension between benzene and water in the presence of caprolactam. J. Colloid Interface Sci. 382 (1), 105–109.
Ullmann's Encyclopedia of Industrial Chemistry, 2000. Wiley-VCH Verlag GmbH & Co. KGaA, Weinheim, Germany.
van Delden, M.L., Kuipers, N.J.M., de Haan, A.B., 2004. Liquid−liquid equilibria and physical properties of the quaternary systems water+caprolactam+ammonium sulfate+benzene and toluene. J. Chem. Eng. Data 49 (6), 1760–1770.
Vandelden, M., Kuipers, N., Dehaan, A., 2006. Selection and evaluation of alternative solvents for caprolactam extraction. Sep. Purif. Technol. 51 (2), 219–231.
Velázquez, M.E., Gama-Goicochea, A., González-Melchor, M., Neria, M., Alejandre, J., 2006. Finite-size effects in dissipative particle dynamics simulations. J. Chem. Phys. 124 (8), 084104.
Wijtkamp, M., van Bochove, G.H., de Loos, Th.W., Niemann, S.H., 1999. Measurements of liquid–liquid equilibria of water+ε-caprolactam+electrolyte+organic solvent systems. Fluid Phase Equilib 158–160, 939–947.